

## Lower-Temperature Pyrolysis to Prepare Biochar from Agricultural Wastes and Adsorption for Pb<sup>2+</sup>

Chunyan Zhang,<sup>a,b</sup> Chunxia He,<sup>a,\*</sup> and Yinhu Qiao<sup>b</sup>

Many agricultural activities generate large quantities of biomass wastes. Using these wastes to produce value-added products or energy has become very important in recent years. Heavy metals such as lead are among the most toxic chemical water pollutants from natural or anthropogenic sources. The goals of this work were to prepare three biochars from maize straw (BMS), sunflower straw (BSS), and wheat straw (BWS) under partial limited oxygen condition and to characterize their ability to adsorb Pb<sup>2+</sup> from water. The sorption kinetics as well as the influence of solution pH and Pb<sup>2+</sup> concentration was investigated. The three biochars had a good performance for Pb<sup>2+</sup> adsorption. A greater adsorption efficiency was observed for BMS and BSS than for BWS. The physico-chemical properties of the biochars showed that the adsorption performance was correlated with preparation conditions, raw material types, higher total porosity, and micro-structure.

*Keywords:* Agricultural wastes; Biochar; Lower-temperature pyrolysis; Partial limited oxygen; Adsorption

*Contact information:* a: College of Engineering Nanjing Agriculture University, Nanjing 210031, China; b: School of Mechanical Engineering, Anhui Science and Technology University, Fengyang 233100, China; \*Corresponding author: chunxiahe@tom.com

### INTRODUCTION

Sorption is an effective method for the removal of metals from water. Activated carbon and biochar have been developed for this purpose. Activated carbon often shows superior performance as an adsorbent for heavy metal ions because of its rich pore structure and large specific surface area. However, the activation process is complex and introduces acidic or alkaline salts, which can be regarded as pollutants. Thus, biochar is a promising sorbent due to its environmental friendliness (Tan *et al.* 2016). Biochar requires a lower investment than conventional activated carbon, which makes it more sustainable. The accumulation of agricultural wastes (AW) and their burning for disposal is a major global environmental problem (Sobati *et al.* 2016), which has prompted the study of biochar made from agricultural wastes. In general, biochar is produced by pyrolysis under oxygen-limited conditions between 200 °C and 800 °C (Chen *et al.* 2016), but the major problem holding back the commercialization of biochar is the complexity of the process (Liu *et al.* 2015). This complexity is mainly related to the necessity of oxygen-limited conditions, which are achieved by evacuating or introducing an inert gas (*i.e.*, N<sub>2</sub>, Ar.). In addition, the required higher pyrolysis temperature increases the cooling time (Jung *et al.* 2016).

The aim of this work was to prepare biochar under a partial limited oxygen environment at a lower temperature. In this study, maize straw (MS), sunflower straw (SS), and wheat straw (WS) were employed as the raw materials for biochar production. The biochar produced in a partial limited oxygen environment at lower temperature

demonstrated good adsorption of  $\text{Pb}^{2+}$  from water with different concentrations of  $\text{Pb}^{2+}$ . The adsorption performance of the biochar derived from maize straw (BMS) and sunflower straw (BSS) was better than that produced from wheat straw (BWS).

## EXPERIMENTAL

### Materials and Equipment

Sunflower straw, maize straw, and wheat straw, which are by-products of agricultural crops, were harvested from Yuling, China, dried at 80 °C for 72 h in a blast oven (DHC-9053A, DAOHAN Industrial Co., Ltd., Shanghai, China), and crushed to 1 to 2 mm by a powder machine. The dry solids were sealed in a vacuum bag for carbonization.

Raw materials of about 25 g from sunflower straw, maize straw, and wheat straw were sealed in a crucible ( $\phi 90 \times 45$ ) and pyrolyzed in a box-type resistance furnace (SX-25-10, Shanghai Boluo Laboratory Equipment Co., Ltd., Shanghai, China) at 300 °C ( $10 \text{ }^\circ\text{C}/\text{min}^{-1}$ ) for 45 min. The products resulting from sunflower straw, maize straw, and wheat straw were named BSS, BMS, and BWS, respectively; the yield for all samples was more than 30%. After cooling, the BSS, BMS, and BWS were sealed in vacuum bags.

### Methods

The three types of carbon were characterized by several techniques. The proximate analysis of the samples was conducted by thermogravimetry (TG) coupled with a differential scanning calorimetry (DSC) (STA449F3, NETZSCH, Selbe, Germany), as previously described (Rashidi *et al.* 2012; Chowdhury *et al.* 2016a). In the TG analysis, 5 to 10 mg of each powder sample was sealed into a ceramic crucible ( $\Phi 8 \times 5$ ) and heated under a 5 mL/min  $\text{N}_2$  flow at 1300 °C with a heating rate of 10 °C/min. The phase identification of the samples was analyzed by X-ray diffraction (XRD) (X'Pert PRO, Almelo, Holland) (Chand *et al.* 2008). The morphology of the samples was characterized by scanning electron microscopy (SEM) (Zeiss EVO18, Oberkochen, Germany) (Chand *et al.* 2009).

The Water Absorption Performance (WAP) is also referred to as the water holding capacity. According to EBC guidelines (DIN ISO 14238-2011), 5~10 g of the three biochars were immersed in water for 24 h, and then the three samples were placed on a sand-bed heaped by napkins for 2 h to remove excess water, respectively. Then, the saturated samples were weighed, dried at 40 °C, and then weighed again.

Surface functional groups were identified by Fourier transform infrared spectroscopy (FTIR) analysis (Nicolet iS-10, Thermo Fisher Scientific). The samples were dried and crushed with KBr. The sample mixed with KBr was pressed to form transparent sheets. Spectra were measured in the range between  $400 \text{ cm}^{-1}$  and  $4000 \text{ cm}^{-1}$ . Basic properties (apparent density, total porosity analysis, *etc.*) of three biochars were measured by high precision density tester (LH-120YE, Xiamen Qunlong Instrument Co., Ltd, Xiamen, China). The distilled water was added to the density meter sink up to the mark. From 5 to 10 g of the biochar was put into a weighing pan and the weight was recorded. Then the material was immersed in water and kept immersed for about 3 s. Then the samples was taken out, wiped off, and placed into the weighing pan again. Finally, the result was read from the instrument.

The surface area and pore sizes in the pyrolyzed biochar were determined by the multipoint N<sub>2</sub> adsorption-desorption method at -196.15 °C using a surface area and pore size analyzer (JW-BK132F, Beijing Micro High-Bo Ltd., Beijing, China) (Li *et al.* 2013).

The adsorption for Pb<sup>2+</sup> in the pyrolyzed biochar was measured by atomic absorption spectrometer (SOLAAR M6, Thermo Fisher Scientific, Waltham, MA, USA) (Li *et al.* 2013). Kinetic adsorption and the effect of initial pH on the adsorption of Pb<sup>2+</sup> on biochar were included in adsorption experiments. For kinetic adsorption, Pb<sup>2+</sup> stock solution (400 mg•L<sup>-1</sup>), using 0.01 mol•L<sup>-1</sup> NaNO<sub>3</sub> as background electrolyte, was prepared by dissolving Pb(NO<sub>3</sub>)<sub>2</sub> in deionized water. The pH of the Pb<sup>2+</sup> solutions was adjusted to 5.0±0.2 by adding 0.1 mol•L<sup>-1</sup> HNO<sub>3</sub> and NaOH solutions. The sorption equilibrium was attained by shaking 0.1 g of biochar in 20 mL of working solution at 180 rpm in a shaker at 25±1°C for 5, 15, 30, and 60 min and 2, 4, 8, and 12 h, respectively. Concentrations of Pb<sup>2+</sup> were measured after the adsorption, the solution was filtered through a 0.45µm syringe filter, and diluted with 1% HNO<sub>3</sub>. The Lagergren pseudo-first-order kinetic model, pseudo-second-order kinetic model and intraparticle diffusion model were used to fit the kinetic adsorption results. The formulas employed are given in Eqs. 2, 3, and 4.

$$\lg(Q_e - Q_t) = \lg Q_e - k_1 t / 2.303 \quad (2)$$

$$\frac{t}{Q_t} = \frac{1}{k_2 Q_e^2} + \frac{t}{Q_t} \quad (3)$$

$$Q_t = k_p t^{0.5} + C \quad (4)$$

where  $k_1$  (h<sup>-1</sup>),  $k_2$  (mg•g•h<sup>-1</sup>), and  $k_p$  (mg•g•h<sup>-0.5</sup>) are quasi-first-order, quasi-second-order rate constants, and intraparticle diffusion coefficients, respectively,  $t$  is reaction time (h),  $Q_t$  and  $Q_e$  are the adsorption amount corresponding to time  $t$  and the adsorption amount when adsorbed (mg•g<sup>-1</sup>), respectively. For the effect of the initial pH value of the solution on the adsorption of Pb<sup>2+</sup> by biochar, Pb<sup>2+</sup> stock solutions (400 mg•L<sup>-1</sup>) was prepared by dissolving Pb(NO<sub>3</sub>)<sub>2</sub> in deionized water. The pH of the Pb<sup>2+</sup> solutions was adjusted to 2.5, 3.5, 4.5, and 5.5 by adding 0.1 mol•L<sup>-1</sup> HNO<sub>3</sub> and NaOH solutions. The sorption equilibrium was attained by shaking 0.1 g of biochar in 20 mL of Pb<sup>2+</sup> solutions with pH 2.5, 3.5, 4.5, and 5.5 respectively at 180 rpm in a shaker at 25±1°C for 24 h. Concentrations of Pb<sup>2+</sup> were measured after the adsorption, the solution was filtered through a 0.45µm syringe filter, and diluted with 1% HNO<sub>3</sub> (Wang and Liu 2017; Zama *et al.* 2017).

## RESULTS AND DISCUSSION

### TG Analysis

TG curves were utilized to analyze the mass loss of raw materials with temperature. The TG and DTG curves are shown in Figs. 1a, b, and c. The process was divided into three stages. The initial stage of the TG graph shows the moisture and volatile substance of the three types of carbons in sunflower straw, maize straw, and wheat straw. The moisture content reflects the water retained by physical bonds only, and intrinsic and extrinsic moisture are the two basic kinds of moisture available. The extrinsic moisture is affected by the weather conditions, yet the intrinsic moisture is the moisture content of the material itself (Cox *et al.* 2002). The second stage of the curves included the loss of the volatile substances and organics. The biomass composition (*i.e.*, cellulose, hemicelluloses,

and lignin) were reduced in this stage. While hemicelluloses and cellulose start to degrade at 220 °C and 300 °C, respectively, lignin degrades gradually in a wider temperature range (Pazó *et al.* 2010). Manahim *et al.* (2011) reported that the temperature ranges for the degradation of hemicellulose, cellulose, and lignin are 250 °C to 320 °C, 320 °C to 380 °C, and room temperature to 900 °C, respectively. The third stage of the curves represents a slow decline to a stable char residual composition. The fixed carbon is calculated from the flat mass region of TG curve after reaching equilibrium temperature. However, the yield of biochar under different temperature was calculated using Eq. 1,

$$Q = \frac{m_2}{m_1} \times 100 \% \quad (1)$$

where  $m_1$  and  $m_2$  are the mass (g) of sunflower straw, maize straw, and wheat straw before and after carbonization, respectively, and  $Q$  is the biochar yield of sunflower straw, maize straw, and wheat straw (%).

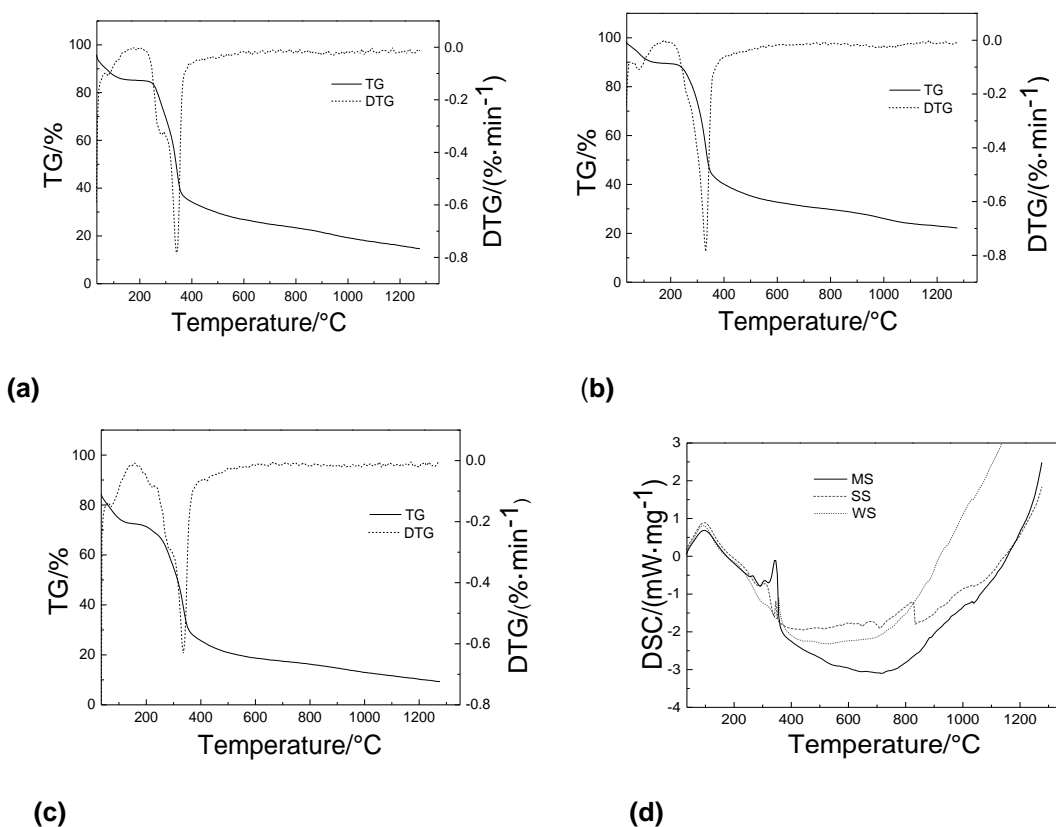


**Fig. 1.** Proximate analysis of the biochars from (a) maize straw (MS), (b) sunflower straw (SS), and (c) wheat straw (WS); (d) differential scanning calorimetry of MS, SS, and WS

The biochars from the sunflower straw, maize straw, and wheat straw had pronounced effects on the development of the volatile substances, ash, and formed biochar, as shown in Figs. 1a, b, and c. When the temperature increased to 100 °C, there were noticeable weight losses. As the temperature reached 200 °C, the biochar contents were expected to increase and the volatile matters to decrease due to pyrolysis. However, a large area of decomposition occurred between 280 °C and 300 °C. When the temperature was

increased further, the volatile substances were gradually released as gases. The weight remained stable after 700 °C, which indicated that the volatile substances and organics were removed (Chowdhury *et al.* 2016b). These results coincide with those reported by Lua and Guo (1998), who proposed that the proximate analysis of the activated carbon could be determined by the nature of the feedstock and operating conditions. In general, the results acquired in this study were comparable with previous reports.

### X-Ray Diffraction Analysis

A comparison of XRD patterns between the biochars and raw materials from sunflower straw, maize straw, and wheat straw is shown in Fig. 2. The XRD patterns of sunflower straw, maize straw, and wheat straw before pyrolysis exhibited two more significant peaks at around  $2\theta = 16^\circ$  and  $22^\circ$ , which mainly were related to the crystalline structure of cellulose in raw materials (Keiluweit *et al.*, 2010). For the three biochars (BMS, BSS, and BWS) prepared at 300°C, the peak near at  $2\theta = 16^\circ$  disappeared, and the peak around  $22^\circ$  showed a broadening tendency, which indicated degradation of cellulose components (Liou and Wu 2009). The XRD patterns of BMS, BSS, and BWS exhibited a significant peak near at  $2\theta = 28.3^\circ$ , being mainly a signal peak of  $\text{CaCO}_3$ , which indicated that the three biochars contained high ash content. In addition, there was a significant peak near at  $2\theta = 40.5^\circ$ , which was signal peak potassium salt (Kim *et al.* 2012). In other words, the three feedstocks of maize straw, wheat straw, and sunflower straw might have undergone a similar transformation process in pyrolysis.

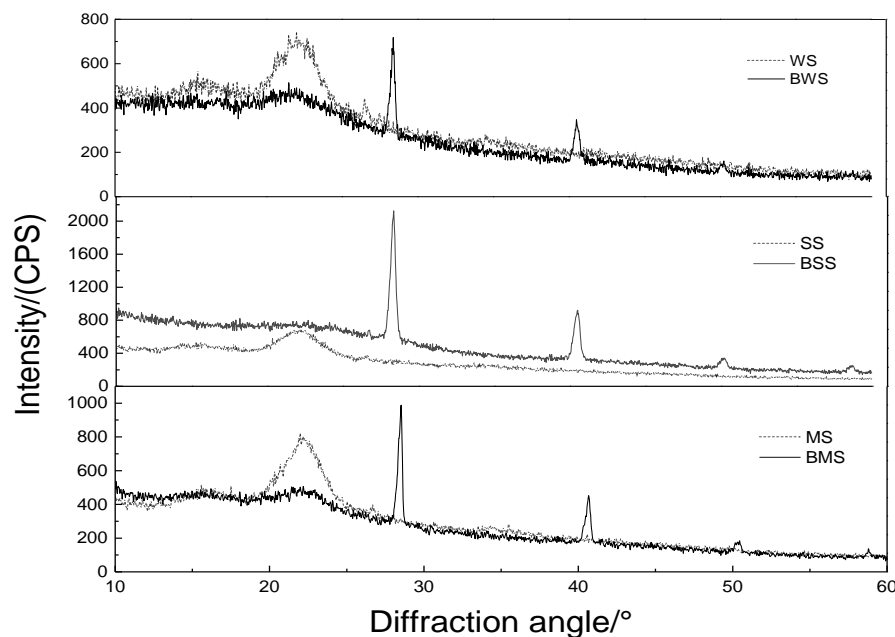
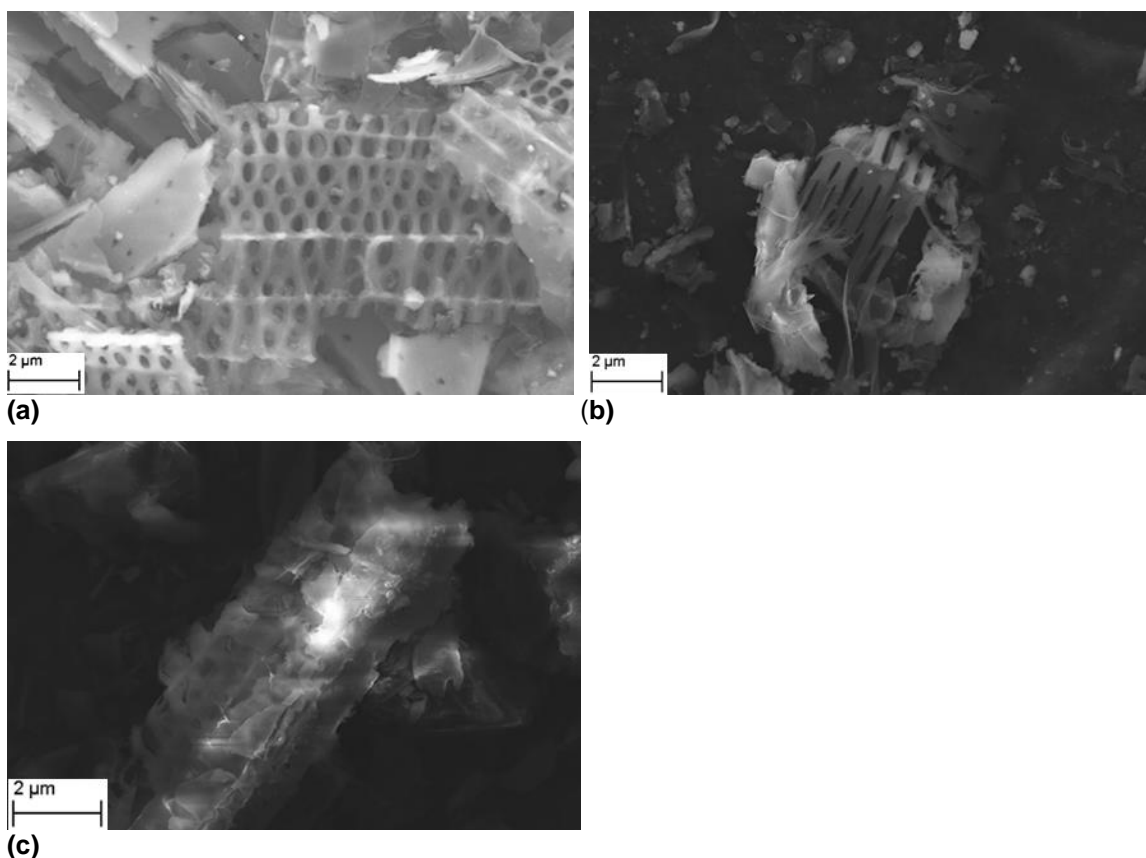


Fig. 2. The comparison of XRD patterns between the biochars and raw materials

### Surface Morphologies

The SEM images of the samples in Fig. 3 show the differences in surface morphology. The biochar surfaces contained pores. There were more pores or cracks in the BMS, which had a larger surface area because of high porosity. Therefore, the raw materials were the main reason of the difference in the surface area and micropore area of biochars. The results are consistent with the porosity analysis in Table 1.



**Fig. 3.** Surface morphologies of the biochars from (a) maize straw (BMS), (b) sunflower straw(BSS), and (c) wheat straw(BWS)

**Table 1.** Basic Properties of Three Biochars

Biochar	Yield (%)	Bulk Specific Gravity (g/cm <sup>3</sup> )	Apparent Density (g/cm <sup>3</sup> )	Apparent Porosity (%)	Water Absorption Rate (%)	Total Porosity (%)
BMS	47.76	0.2181	0.259	15.62	71.43	92.78
BSS	48.97	0.2210	0.230	3.77	17.02	92.63
BWS	40	0.2322	0.245	4.79	20.59	92.20

### Fourier Transform Infrared Spectroscopy

To determine the change of functional groups, the FTIR spectra of sunflower straw, maize straw, and wheat straw before and after pyrolysis are shown in Fig. 4. The main absorption peaks of samples appeared in the wavenumber region between 500 cm<sup>-1</sup> and 2000 cm<sup>-1</sup>. Generally, the C=O stretching vibration in the carboxyl group appeared at 1706 cm<sup>-1</sup>. The characteristic peak interval of benzene ring or aromatic was at 1450 cm<sup>-1</sup> to 1610 cm<sup>-1</sup>. The absorption peaks that are representatives of C=O stretching vibrations, C=C stretching, and the -OH out-of-plane bending vibration of phenols, ethers, and alcohols appeared at 1102 cm<sup>-1</sup> to 1252 cm<sup>-1</sup>. The absorption peak of the aromatic compound C-H was at 793 cm<sup>-1</sup>. Compared to raw materials, the absorption peaks of biochars were reduced clearly at 1102 cm<sup>-1</sup> to 1252 cm<sup>-1</sup>. This result indicated that the samples with different feedstocks before and after pyrolysis had hydroxyl, aromatic, and some oxygen-containing functional groups, but the absorption intensity was somewhat different. And the reason of the absorption peaks being reduced clearly at 1102 cm<sup>-1</sup> to 1252 cm<sup>-1</sup> after pyrolysis was

mainly that the -OH functional groups of phenols, ethers, and alcohols of raw materials disappeared with temperature increasing. The results were similar to other biochars (Sardella *et al.* 2015).

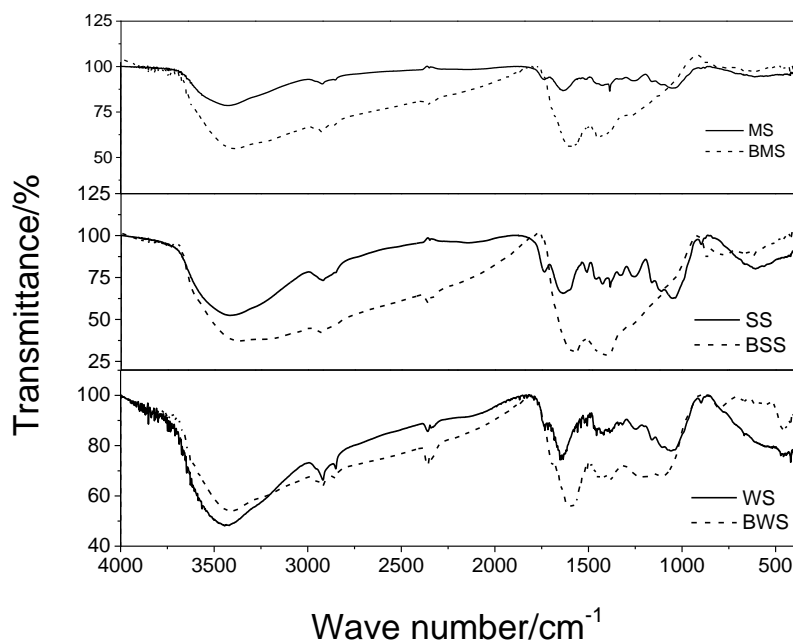


**Fig. 4.** FTIR spectra of the biochars from sunflower straw, maize straw, and wheat straw

### The Surface Area and Pore Size Analysis

The specific surface area and total pore volume of the BMS, BSS, and BWS are shown in Table 2. The specific surface area and total pore volume of the three biochars were all lower. BSS had the highest values of specific surface area and total pore volume at  $5.61552 \text{ m}^2/\text{g}$  and  $0.00908 \text{ m}^3 \cdot \text{g}^{-1}$ , respectively. Compared to active carbon of better adsorbent, the specific surface area and total pore volume of the three biochars were much lower. Generally, the specific surface area and total pore volume are main indicators to measure the adsorption performance of materials. However, these results showed that the specific surface area and total pore volume had little influence on adsorption performance of the three samples (Yang *et al.* 2015).

**Table 2.** Specific Surface Area, Total Pore Volume, and Average Pore Size of Three Biochars

Type	BMS	BSS	BWS
Specific surface area/ $\text{m}^2 \cdot \text{g}^{-1}$	4.15224	5.61552	2.48631
Total pore volume/ $\text{m}^3 \cdot \text{g}^{-1}$	0.00682	0.00908	0.00394

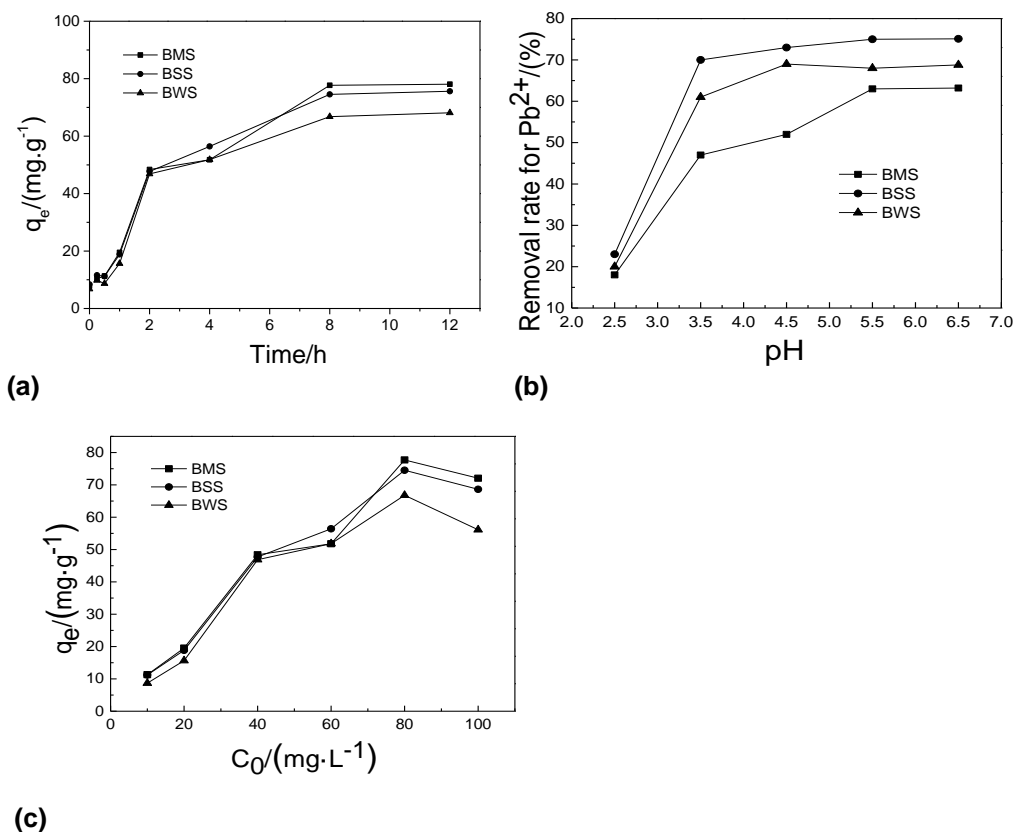
### The Adsorption Performance for $\text{Pb}^{2+}$

Figure 5a presents the effect of contact time on  $\text{Pb}^{2+}$  adsorption by BMS, BSS, and BWS. The adsorption of  $\text{Pb}^{2+}$  by three biochars all reached equilibrium adsorption by around 8 h. The intraparticle diffusion model was used to fit the adsorption results. The

results showed that BMS and BSS had better fitting effect for  $\text{Pb}^{2+}$  adsorption, which the value of  $R^2$  were 0.93236 and 0.92118, respectively.

The pH is one of the most important environmental factors influencing the dissociation of surface functional groups and the solution chemistry of metals (Sardella *et al.* 2015). Figure 5b presents the effect of pH on the removal of  $\text{Pb}^{2+}$  by BMS, BSS, and BWS. The amount adsorbed increased sharply with increasing pH, reaching the equilibrium quantities at pH 5.0 for  $\text{Pb}^{2+}$ . The values were similar for all adsorbents studied in this work and are comparable to those found in the literature (Li *et al.* 2014; Li *et al.* 2015).

Taking into account these results, kinetic adsorption assays for  $\text{Pb}^{2+}$  were developed by adjusting the suspension initial pH to over 5.5 (Bogusz *et al.* 2015). Figure 5b shows the kinetic curves obtained for  $\text{Pb}^{2+}$  adsorption assays using BMS, BSS, and BWS. In all cases the maximum removal amount was achieved when the initial concentration of  $\text{Pb}^{2+}$  was 80 mg/L, as shown in Fig. 5c. Figure 5c shows that BMS had a better performance in  $\text{Pb}^{2+}$  adsorption than the other two biochars. In this case, BSS and BWS showed an improved performance in  $\text{Pb}^{2+}$  adsorption, reaching 94.83% and 80.98% of metal removal, respectively. Compared to the study by Tekin *et al.* (2016), the three biochars had much lower specific surface areas and total pore volume, but the adsorption to  $\text{Pb}^{2+}$  was as good as the cited study. It is apparent that the porous structure had some influence on metal retention. The difference in adsorption performance of biochars were mainly caused by surface chemical groups of biochars (Sardella *et al.* 2015).



**Fig. 5.** The effect of biochars from (a) contact time on  $\text{Pb}^{2+}$  adsorption, (b) pH influence on  $\text{Pb}^{2+}$  adsorption, and (c)  $\text{Pb}^{2+}$  adsorption isotherms

## CONCLUSIONS

1. The surface area and micropore area of biochars were mainly determined by the raw materials.
2. A biochar with the highest total porosity of 92.8% and the maximum removal of Pb<sup>2+</sup> adsorption of 98.3% (78.6 mg/g) was produced from maize straw at the temperature of 300 °C under partial limited oxygen condition.
3. The low-temperature pyrolysis and the partial limited oxygen condition process that was used to carbonize sunflower straw, maize straw, and wheat straw was feasible and beneficial to the recycling of agricultural wastes, which simplified the preparation of carbon adsorbents.

## ACKNOWLEDGMENTS

The authors thank the following for their support of this work: the Key Project Supported by Foundation University of Science and Technology of Anhui (No. JXWD201602 and ZRC2016492), the Project Supported by Anhui Science and Technology Department (No. KJ2018A0536, 1704a0902058, KJ2017ZD44, KJ2015A195, 1708085QD85, gxyqZD2016213 and 1704e1002238), the Key Construction Disciplines Project Supported by University of Science and Technology of Anhui (No. AKZDXK2015C03), and the Project Supported by the National Natural Science Foundation of China (No. 21607002, 2017YFD0200808).

## REFERENCES CITED

- Bogusz, A., Oleszczuk, P., and Dobrowolski, R. (2015). "Application of laboratory prepared and commercially available biochars to adsorption of cadmium, copper and zinc ions from water," *Bioresource Technol.* 196, 540-549. DOI: 10.1016/j.biortech.2015.08.006
- Chand, R., Watari, T., Inoue, K., Torikai, T., and Yada, M. (2008). "Evaluation of wheat straw and barley straw carbon for Cr (VI) adsorption," *Sep. Purif. Technol.* 65(3), 331-336. DOI: 10.1016/j.seppur.2008.11.002
- Chand, R., Watari, T., Inoue, K., Kawakita, H., Luitel, H. N., Parajuli, D., Torikai, T., and Yada, M. (2009). "Selective adsorption of precious metals from hydrochloric acid solutions using porous carbon prepared from barley straw and rice husk," *Miner. Eng.* 22(15), 1277-1282. DOI: 10.1016/j.mineng.2009.07.007
- Chowdhury, Z. Z., Hamid, S. B., Rahman, M. M., and Rafique, R. F. (2016a). "Catalytic activation and application of microspherical carbon derived from hydrothermal carbonization of lignocellulosic biomass: Statistical analysis using Box-Behnken design," *RSC Advances* (6), 102680-102694. DOI: 10.1039/c5ra26189a
- Chowdhury, Z. Z., Karim, M. Z., Ashraf, M. A., and Khalid, K. (2016b). "Influence of carbonization temperature on physicochemical properties of biochar derived from slow pyrolysis of durian wood (*Durio zibethinus*) sawdust," *BioResources* 11(2), 3356-3372. DOI: 10.15376/biores. 11.2. 3356 -3372

- Cox, P. M., Betts, R. A., Betts, A., Jones, C. D., Spall, S. A., and Totterdell, I. J. (2002). "Modeling vegetation and the carbon cycle as interactive elements of the climate system," *Int. Geophysics* 83, 259-279. DOI: 10.1016/S0074-6142(02)80172-3.
- Chen, D., Yu, X., Song, C., Pang, X., Huang, J., and Li, Y. (2016). "Effect of pyrolysis temperature on the chemical oxidation stability of bamboo biochar," *Bioresource Technol.* 218, 1303-1306. DOI: 10.1016/j.biortech.2016.07.112
- Jung, K. W., Jeong, T. U., Kang, H. J., and Ahn, K. H. (2016). "Characteristics of biochar derived from marine macroalgae and fabrication of granular biochar by entrapment in calcium-alginate beads for phosphate removal from aqueous solution," *Bioresource Technol.* 211, 108-116. DOI: 10.1016/j.biortech.2016.03.066.
- Keiluweit, M., Nico, P. S., Johnson, M. G., and Kleber, M. (2010). "Dynamic molecular structure of plant biomass-derived black carbon (biochar)," *Envir. Sci. Technol.* 44, 1247-1253. DOI: 10.1021/es9031419.
- Kim, K. H., Kim, J. Y., Cho, T. S., and Choi, J. W. (2012). "Influence of pyrolysis temperature on physicochemical properties of biochar obtained from the fast pyrolysis of pitch pine (*Pinus rigida*)," *Bioresource Technol.* 118, 158-162. DOI: org/10.1016/j.biortech.2012.04.094.
- Li, K. Q., Li, Y., Zheng, Z., and Sang, D. Z. (2013). "Preparation, characterization, and adsorption performance of high surface area biomass-based activated carbons," *Envir. Sci.* 34(1), 328-335. DOI: 10.13227/j.hjkx.2013.01.042
- Li, K. Q., Wang, Y. J., Yang, M. R., Zhu, Z. Q., and Zheng, Z. (2014). "Adsorption kinetics and mechanism of lead(II) on polyamine-functionalized mesoporous activated carbon," *Envir. Sci.* 35(8), 3198-3205. DOI: 10.13227/j.hjkx.2014.08.051
- Li, R. Y., Chen, D., Li, L. Q., Pan, G. X., Chen, J. Q., and Guo, H. (2015). "Adsorption of Pb<sup>2+</sup> and Cd<sup>2+</sup> in aqueous solution by biochars derived from different crop residues," *J. Agro-Environment Sci.* 34(5), 1001-1008. DOI: 10.11654/jaes.2015.05.025
- Liou, T. H., and Wu, S. J. (2009). "Characteristics of microporous/mesoporous carbons prepared from rice husk under base and acid-treated conditions," *J. Hazard. Mater.* 171(1-3), 693-703. DOI: 10.1016/j.jhazmat.2009.06.056.
- Lua, A. C., and Guo, J. (1998). "Preparation and characterization of chars from oil palm waste," *Carbon* 36(11), 1663-1670. DOI: 10.1142/9789812791924\_0077.
- Liu, N., Charrua, A. B., Weng, C. H., Yuan, X. L., Ding, F. (2015). "Characterization of biochars derived from agriculture wastes and their adsorptive removal of atrazine from aqueous solution: A comparative study," *Bioresource Technol.* 198, 55-62. DOI: 10.1016/j.biortech.2015.08.129
- Pazó, J. A., Granada, E., Saavedra, Á., and Collazo, J. (2010). "Uncertainty determination methodology, sampling maps generation, and trend studies with biomass thermogravimetric analysis," *Int. J. Mol. Sci.* 11(10), 3660-3674. DOI: 10.3390/ijms11103660
- Rashidi, N. A., Yusup, S., Ahmad, M. M., Mohamed, N. M., and Hameed, B. H. (2012). "Activated carbon from the renewable agricultural residues using single step physical activation: A preliminary analysis," *APCBEE Procedia* 3(6), 84-92. DOI: 10.1016/j.apcbee.2012.06.051
- Sardella, F., Gimenez, M., Navas, C., Morandi, C., Deiana, C., and Sapag, K. (2015). "Conversion of viticultural industry wastes into activated carbons for removal of lead and cadmium," *J. Envir. Chem. Eng.* 3, 253-260. DOI: 10.1016/j.jece.2014.06.026

- Sobati, M. A., Hajamini, Z., Shahhosseini, S., and Ghobadian, B. (2016). "Waste fish oil (WFO) esterification catalyzed by sulfonated activated carbon under ultrasound irradiation," *Appl. Therm. Eng.* 94, 141-150. DOI: 10.1016/j.applthermaleng.2015.10.101
- Tan, X. F., Liu, Y. G., Gu, Y. L., Xu, Y., Zeng, G. M., Hu, X. J., Liu, S. B., Wang, X., Liu, S. M., and Li, J. (2016). "Biochar-based nano-composites for the decontamination of wastewater: A review," *Bioresour Technol.* 212, 318-333. DOI: 10.1016/j.biortech.2016.04.093.
- Tekin, K., Akalin, M. K., Uzun, L., Karagoz, S., Bektas, S., Denizli, A. (2016). "Adsorption of Pb(II) and Cd(II) ions onto dye-attached sawdust," *CLEAN–Soil, Air, Water* 44(4), 339-344. DOI:10.1002/clen.201500222.
- Wang, Y., and Liu, R. H. (2017). "Comparison of characteristics of twenty-one types of biochar and their ability to remove multi-heavy metals and methylene blue in solution," *Fuel Process. Technol.* 160, 55-63. DOI: 10.1016/j.fuproc.2017.02.019.
- Yang, J. B., Yu, M. Q., and Chen, W. T. (2015). "Adsorption of hexavalent chromium from aqueous solution by activated carbon prepared from longan seed: Kinetics, equilibrium, and thermodynamics," *J. Ind. Eng. Chem.* 21(1), 414-422. DOI: org/10.1016/j.jiec.2014.02.054.
- Zama, E. F., Zhu, Y.-G., Reid, B. J., and Sun, G. X. (2017). "The role of biochar properties in influencing the sorption and desorption of Pb(II), Cd(II) and As(III) in aqueous solution," *J. Clean. Prod.* 148, 127-136. DOI: org/10.1016/j.jclepro.2017.01.125.

Article submitted: September 3, 2017; Peer review completed: October 15, 2017; Revised version received and accepted: May 10, 2018; Published: June 4, 2018.  
DOI: 10.15376/biores.13.3.5543-5553